A fast yet force-effective mode of collective cell migration on aligned fibers due to rapid stabilization of contractile forces

Authors: Amrit Bagchi[1], Bapi Sarker[1], Jialiang Zhang[2], Marcus Foston[2], Amit Pathak[1,*]

Affiliations: [1]*Department of Mechanical Engineering & Materials Science,* [2]*Department of Energy, Environmental & Chemical Engineering, Washington University, St. Louis*

*To whom correspondence should be addressed:
Amit Pathak, Ph.D.
One Brookings Dr., CB 1185, Saint Louis, MO 63130
Ph: (314) 935-7585; Email: pathaka@wustl.edu

Abstract:

Cell collectives use aligned extracellular matrix fibers for directed migration in development, regeneration, and cancer metastasis. Previously, stiffer matrices and aligned matrix topographies have been shown to independently enhance and polarize cellular forces, which in turn speed up cell migration. However, it remains unknown whether fibers serve as active conduits for spatial propagation of cellular mechanotransduction and directed collective cell migration independently of stiffness cues. In this work, we developed soft hydrogels coated with magnetically aligned collagen fibers and studied migration of defined epithelial clusters. We report that epithelial (MCF10A) cell clusters adhered to soft substrates with aligned collagen fibers (AF) migrate faster with much lesser traction forces, compared to those on uniform fibers (UF). Fiber alignment causes motility and force transmission deeper into the monolayer, leading to polarized cell flocking, compared to migration on UF where cellular jamming occurs. Using a motor-clutch model, we explain that force-effective fast migration phenotype occurs due to faster stabilization of cellular contractile forces enabled by aligned ligand connectivity. As a result, cells migrate faster with lesser effort, thereby revealing that aligned matrix topographies may help conserve energy for cell migration in fundamental biological processes such as wound repair and tumor invasion.

Significance statement:

Cellular forces are critical for their collective migration on matrices of varies stiffness and topographies. While cells can align collagen fibers during migration, it remains unknown whether such force requirement changes with pre-aligned fibers. On soft surfaces with aligned collagen fibers, we discovered a new mode of fast collective cell migration that requires drastically lower traction forces, compared to surfaces without aligned fibers. Through monolayer stress microscopy calculations and a motor-clutch model, we further discovered that this novel mode of “fast and force-effective” collective cell migration is achieved by rapid stabilization of cellular contractile forces. Although high traction forces have conventionally been associated with fast cell migration, our findings show that aligned fibers relax that force requirement via contractility stabilization.

Main Text:

Directed collective cell migration is ubiquitous in fundamental processes like organ development and regeneration (*1*), (*2*). However, physical or biochemical mechanisms that dictate mesoscopic order across supra-cellular length scales are not well understood. Mechanistically, large-scale propagation of mechanical signals leading to directionally cooperative behavior has been recognized, but not yet elucidated. Recently, collective cells undergoing directional migration on substrates having gradients in stiffness (durotaxis) have shown to utilize long range force propagation (*3*) aided via underlying substrate, motivating a hypothesis that efficient signal transduction could be a key component in explaining directional migration. Thus, it is possible that if extracellular force propagation works in coordination with mechanical stress transfer across cell-cell junctions, such cooperation could generate more efficient collective cell migration. This is an intriguing possibility given that force transfer across cellular junctions correlates only to a limited spatial extent in unbiased migration, thereby reducing migration efficiency.

Directional collective migration via contact guidance in the form of aligned extracellular matrix (ECM) fibers is critical in tissue healing and regenerations (*4*)–(*6*) as well as a strong regulator of carcinoma progression (*7*)–(*10*). There have been extensive studies on parallel grooves or adhesive ligands aimed at mimicking this phenomenon in 2D (*11*)–(*14*). While these studies have focused on capturing ligand continuity in a particular direction by uniformly coating ligands along the topography or adhesive strip, the fact that ligands on aligned fibers *in vivo* are connected to each other and can potentially serve as sources of large-scale propagation of mechanical signals has not yet been investigated. This gap in knowledge provides us with an opportunity to test our hypothesis of extra-cellular force propagation via aligned fibers as an adjuvant to mechanical stress transfer across cellular junctions helping cellular cohorts to exhibit directional migration in aligned fibrous microenvironments.

To probe the above hypothesis, we develop an experimental approach where we use aligned collagen-1 fibers as directional cues for cell migration on soft 2D surfaces that mimic physiological stiffness. We first synthesize modified soft polyacrylamide (mod-PA) hydrogels, which enable attachment of tunable collagen fibers, as previously described (*15*). We then incubate these hydrogels in a collagen-1 solution (0.1 mg/ml) and expose to a high-strength magnetic field (11 T) during collagen fibrillogenesis at 4° C (Fig. 1b, Fig. S1a) (*16*). During this process, collagen fibers settle and covalently attach to the gels, with alignment along a desired direction (*15*). Next, using magnetic polydimethyl-siloxane (PDMS) stencils, we micro-patterned rectangular clusters (500 µm wide) of human mammary epithelial cells (MCF-10A) on these aligned collagen-coated mod-PA gels in a manner such that directions of leading edge advancement and collagen alignment are parallel (Fig 1a). We measure the effect of collagen alignment on collective migration by comparing it against uniformly distributed collagen fibers without alignment bias. To achieve uniformly coated collagen surfaces, mod-PA gels were incubated with collagen solution at 37° C, without magnetic field, followed by cell cluster patterning (Fig. 1c, Fig. S1b) (*15*).

Upon removal of the PDMS stencil, rectangular cell clusters expanded symmetrically on both aligned fiber gels (AF) and uniform fiber gels (UF) (Fig. 1 (d, e)). To better understand the large-scale spatiotemporal fluctuations of mechanical patterns within the expanding monolayer, we averaged velocities, tractions, and monolayer stresses across length (y-coordinate), thereby reducing

dimensionality of system to a single spatial dimension (x-axis, which is the also the direction of collagen alignment) and the temporal dimension (Fig. 1 (h-k), 2 (a-d), 3(i-n)). By comparing cell migration trajectories (Fig. 1f-g, Fig. S1c-d), we observed that cell clusters on AF migrated faster (1.8 times) compared to the cells migrating on UF. Additionally, cell clusters migrated more persistently along the x-direction leading to a net higher expansion of the monolayer on AF, indicating that cells were using aligned fibers as directional cues to navigate their migration (Fig S1e). For AF, cell movements were more homogenous with higher velocities at the leading edge penetrating greater depths within the monolayer, compared to a more heterogeneous distribution in UF characterized by outward faster velocities and middle regions with much lesser velocities (Fig. 1h,i). Quantitatively, the spatial velocity autocorrelation function follows a slower spatial decay in AF, confirming that cellular motion is correlated across greater distances when compared to UF (Fig. 1i).

Given the spatial cooperation in migrating cells driven by aligned fibers, we next investigated whether cell movements had differences in temporal heterogeneity across the conditions. We measure this heterogeneity using the four-point susceptibility χ_4, a soft matter physics tool used for measuring the rate of structural rearrangements between any two points in space within a time window. We computed χ_4 from the variance of the self-overlap order parameter (see Methods). While the location of the peak of χ_4 indicates time interval in which cell migration dynamics are highly heterogeneous, the height of the peak denotes the spatial extent of such heterogeneities (*17*). Comparing AF versus UF, there is a distinct shift in χ_4 peak to longer timescales for UF (Fig. 1m), indicating a more jammed state for cells migrating on UF. Additionally, the peak height for UF is higher, indicating larger clusters of jammed cells in UF. According to previous work in inert particulate matter (*18*), (*19*), differences in mutual crowding between the two conditions could be responsible for promoting jamming in one condition over the other. To explore this potential mechanism for the observed jamming differences in AF and UF, we measured cellular areas (Fig. 1n,o) densities (Fig. S1d)and aspect ratios (Fig. 1n, Fig. S1e)) across the two conditions. As shown in figures, cells on UF tended to have a higher area and aspect ratio compared to AF while also having much lesser densities. While cellular morphologies do agree with the notion that cells on UF are in a more jammed state (*20*), it is quite counter-intuitive to find that such a state existed in UF at lesser cellular densities when compared to AF. This is particularly surprising because jamming tends to occur at higher densities in inert systems (*19*), (*21*). This experimental evidence thus helps us to reject a density based jamming hypothesis. For the cells in the x-direction on AF, our analysis suggest a flocking type of migratory phenotype (*22*), (*23*), which is spatially homogenous and temporally dynamic. By contrast, on UF, migration is much more heterogeneous and static. It is possible that these differences in phenotype are a result of homogeneity in ligand orientation on AF and the lack thereof on UF.

Interestingly, for AF alone, there were multiple strain-rate X-waves propagating away from leading edge, coalescing at the middle of the monolayer and then propagating back to the edge (Fig. 1j,k, Fig. 2l,m). This phenomenon was less frequent for UF. Although efficiency of mechanical wave transmission has not been linked to jamming before, the results here do provide evidence to the hypothesis that cell mobilization away from the leading edge is higher and more efficient on AF compared to UF. Interestingly, this transmission takes place across greater number of cell-cell junctions on AF owing to density differences between the two conditions.

121 Experimental results presented thus far suggest that cell clusters on AF migrate with faster
122 velocities. This unjammed migration phenotype also displays an effective relay of motion from the
123 monolayer front to the rear. By contrast, on UF, cells are slower and jammed with a disrupted transmission
124 of motion. Since motion of a collective cohort of cells depends on the effective transfer of stresses across
125 the monolayer (*24*), and while we see effective transfer of motion in only one of the condition, we sought
126 to compare how well forces were getting transmitted across the cells between the conditions. To this end,
127 we first studied traction force evolution within the monolayer. For AF, tractions in x-direction (T_x)
128 kymographs demonstrated much lower (1/5th) traction magnitudes compared to UF (Fig. 2 a,b). Although
129 direct force measurements have not been reported before, this result is surprising because migration
130 studies on stiff substrates in the past have suggested that cells apply higher forces on aligned topographies
131 (*14*). Interestingly, the traction distribution for both conditions was different. While tractions were evenly
132 distributed across the monolayer width on AF, there were heterogeneities in UF, with higher tractions
133 localized at the leading edges, followed by a steep decrease in middle regions. These differences in
134 traction distribution run parallel to the velocity distribution differences seen between the two conditions.

135 Since the T_x kymographs hint at differences in force transmission across the monolayer width
136 between the two fiber alignment conditions, we probe this further by measuring force transmission using
137 monolayer stress microscopy (*25*). Although kymographs for monolayer stress component σ_{xx} for both
138 AF and UF (Fig. 2c,d) showed maxima at the monolayer midline, indicating build-up of stress differentials
139 at the monolayer center via cell-cell junctions, the extent of this build-up was different for both conditions.
140 Cells on AF had one-fifth of the built-up stresses compared to UF (Fig. 2c,d). This difference was also
141 reflected in the average strain energy plots, which show that cells on AF transfer one-fifth of the strain
142 energy to the substrate compared to the UF (Fig. 2q). To examine the extent of stress cooperativity within
143 the monolayer, we also calculated the spatial correlation function (*C(R)*) of the average normal stress. As
144 shown in Fig 2(p), cells on AF exhibit slower spatial decay of *C(R)*, indicating that average normal stresses
145 were correlated over greater distances. Interestingly, according to T_y kymographs, cells on AF apply
146 negligible forces in the y-direction, while cells on UF apply much higher forces that are equivalent to forces
147 in x-direction (Fig. S3c-e). These distinct differences in T_y indicate that cells on AF are polarized along the
148 direction of collagen alignment and predominantly pull along the collagen fibers, while cells on UF apply
149 forces isotropically without a directional bias.

150 Since cellular velocity and stress propagate across the monolayer differently between AF and UF,
151 we next probed the relationship between these two fundamental physical quantities that determine
152 grouped cell behavior. Earlier studies have shown that cells have the tendency to migrate along the
153 direction of minimal shear stress, a phenomenon known as "plithotaxis" (*25*). To check the effect of
154 collagen alignment on plithotaxis, we first rank-ordered the pairs of stress and velocity according to their
155 distances from leading edge into 5 quintiles (Fig. 2g-i). Next, for each quintile, we measured the alignment
156 angle φ between local maximal principal stress orientation and local migration velocity vector orientation.
157 We calculated the cumulative probability distribution of φ for each quintile to assess the extent of
158 alignment between velocity and maximal principal stress. Higher degree of alignment would be associates
159 with a steeper rising curve. In both AF and UF, we observe that moving away from the leading edge causes
160 reduction in alignment between local stress and cellular motion, indicating that plithotaxis is most

161 dominant at the leading edge (Fig. 2r,s). However, for each quintile, AF shows a stronger alignment
162 between stress and velocity (steeper curve) when compared to UF. This indicates that plithotaxis is more
163 dominant in AF at all regions within the monolayer when compared to UF, which supports our hypothesis
164 of an efficient transfer of stresses from front to rear of the migrating monolayer across its cell-cell
165 junctions. This long-distance stress propagation guided by aligned collagen fibers enables a more effective
166 transfer of motion from the leader to the follower population. By contrast, both the front-rear stress
167 propagation and the leader-follower velocity cooperation get disrupted when fibers are uniformly
168 distributed without any preferred orientation.

169 Previously, cytoskeletal fluidization has been shown to regulate dissipation of built-up stresses
170 within cell monolayers for their active expansion (*26*). Here, we measure the extent of fluidization within
171 the monolayer by measuring stress oscillations at the monolayer midline. Multiple stress peaks arise for
172 AF, compared to a single such peak in UF for the entire migration duration (Fig. 2l,m). These periodic built-
173 up and release of stresses at the monolayer midline for AF indicates an efficient long-range stress
174 transmission across cells, a process absent in UF. Additionally, in accordance with previous literature (*26*),
175 these stress oscillations were in a phase quadrature to velocity strain rate oscillations but in phase with
176 cellular area fluctuations (Fig. 2n,o). Given that stresses are more frequently dissipated in AF, it would be
177 indicative of more frequent regulation of cell size, consistent with recent work showing coordination of
178 cell size and stress within a monolayer (*27*). This cell size-stress balancing act could explain why stresses
179 within the monolayer are not allowed to build up, leading to overall lower stresses on AF. On AF, higher
180 frequency of cell shape adaptation results in overall reduction in cell size as stresses are seamlessly
181 transferred across cells. However, on UF, infrequent transfer of stresses leads to stress build-up within
182 the cells, which coincides with increase in cell size.

183 As a confirmation of the above phenotype, we repeated the experiment by further lowering the mod-PA
184 substrate stiffness. We find that cells still migrate faster on AF compared to UF (1.34 times) while applying
185 much lesser forces ($1/4^{th}$) on AF when compared to UF (Fig. S3a,c). We also find that both cellular
186 velocities and stresses are correlated across greater distances in clusters migrating on AF (Fig. S3b,d).
187 Expectedly, we also observed higher spatial extent of plithotaxis in clusters migrating on AF (Fig. S4e-i).

188 Our experimental measurements establish that monolayers use aligned collagen fibers to expand
189 faster while generating lesser contractile tractions and monolayer stresses. Also, we show that these
190 forces are transmitted across greater distances within the cluster. To better understand why fiber
191 alignment leads to faster migration without the need for higher forces, we developed a physical model
192 which incorporates clutch-like cell-ECM interactions in a minimalist framework wherein cell monolayer,
193 collagen fibers, and soft substrate are treated as a collection of elastic springs connected in series (Fig.
194 4a). While UF is modelled as individual ligand springs disconnected from one another, AF is modelled by
195 connecting these ligand springs to each other, depicting ligand connectivity along the direction of
196 migration (Fig. 4b,c).

197 The model predicts a faster cell cluster expansion during its migration over connected ligand
198 springs (compared to the disconnected condition), while generating lesser traction forces on the
199 underlying substrate mesh. Cells within the cluster are also able to fluidize more often when migrating
200 over connected fibers, thus leading to release of build-up stress within the cell cluster. In our model, fiber

connectivity causes engagement of more ligand-substrate bonds as the leading-edge cell node contracts after a protrusion event. This rise in ligand-substrate bonds results in higher load sharing capability amongst the nodes, leading to quicker stabilization of the contracting leading edge. Quicker stabilization further leads to faster subsequent protrusions and overall expansion of the cluster (Fig. 4d,e). Another effect of faster contractility stabilization is reduced retraction of the cell cluster, compared to the disconnected fiber condition, which in turn causes lesser substrate deformation and traction (Fig. 4f,g). As a whole, the faster stabilization of the leading edge on connected fibers causes quicker transfer of stress from the edge to the center, which in turn results in faster stretch-based cell fluidization within the monolayer. However, in case of slower stabilization of cluster edge, the related slower transfer of strains to the center reduces the frequency of fluidization events within the monolayer (Fig. 4h,i).

Given the close agreement between the experiments and model predictions, we conclude that long-range force transmission via connected ligands leads to a more efficient mode of migration in terms of force required to generate migration velocity on matrix conditions that offer higher ligand connectivity. While long-range force transmission as an underlying mechanism for collective directional migration has been alluded to in the past (*3*), our experiments use constant matrix stiffness across conditions, thus keeping stiffness sensitive mechano-transduction pathways within the cells constant and thereby removing the effective contribution of stiffness from directional migration or its effect in long range force transmission. We also speculate that utilizing aligned ECM fibers on 2D substrates gives rise to a quasi-2D mode of contact-guided directional migration, which delineates the role of ligand connectivity as opposed to uniformly coated ligands on micropatterned protein stripes or topographical grooves (*11*), (*13*). Uniform ligand coating leads to ligand continuity but not connectivity, thus restricting matrix mechano-transmission that could take place outside of the cell monolayer. In light of recent evidence of cell division upregulation upon mechanical stretching (*28*), future work could explore how differences in mechanical properties within the monolayer dictates the ease of proliferation-based monolayer fluidization in the presence of ligand connectivity.

228 ## References and Notes:

229 1. A. McMahon, G. T. Reeves, W. Supatto, A. Stathopoulos, Mesoderm migration in Drosophila is a
230 multi-step process requiring FGF signaling and integrin activity. *Development*. ***137***, 2167–2175
231 (2010).

232 2. R. J. Petrie, A. D. Doyle, K. M. Yamada, Random versus directionally persistent cell migration. *Nat.*
233 *Rev. Mol. Cell Biol.* ***10***, 538–549 (2009).

234 3. R. Sunyer *et al.*, Collective cell durotaxis emerges from long-range intercellular force
235 transmission. *Science (80-.).* ***353***, 1157–1161 (2016).

236 4. R. T. Tranquillo, Self-organization of tissue-equivalents: the nature and role of contact guidance.
237 *Biochem. Soc. Symp.* ***65***, 27–42 (1999).

238 5. G. Reig, E. Pulgar, M. L. Concha, Cell migration: from tissue culture to embryos. *Development*.
239 ***141***, 1999–2013 (2014).

240 6. A. Czirok, Endothelial cell motility, coordination and pattern formation during vasculogenesis.
241 *Wiley Interdiscip. Rev. Syst. Biol. Med.* ***5***, 587–602 (2013).

242 7. P. P. Provenzano, D. R. Inman, K. W. Eliceiri, S. M. Trier, P. J. Keely, Contact Guidance Mediated
243 Three-Dimensional Cell Migration is Regulated by Rho/ROCK-Dependent Matrix Reorganization.
244 *Biophys. J.* ***95***, 5374–5384 (2008).

245 8. P. P. Provenzano *et al.*, Collagen density promotes mammary tumor initiation and progression.
246 *BMC Med.* ***6***, 11 (2008).

247 9. P. P. Provenzano, K. W. Eliceiri, J. M. Campbell, D. R. Inman, J. G. White, P. J. Keely, Collagen
248 reorganization at the tumor-stromal interface facilitates local invasion. *BMC Med.* ***4***, 38 (2006).

249 10. M. W. Conklin *et al.*, Aligned collagen is a prognostic signature for survival in human breast
250 carcinoma. *Am. J. Pathol.* ***178***, 1221–1232 (2011).

251 11. S. R. K. Vedula *et al.*, Emerging modes of collective cell migration induced by geometrical
252 constraints. *Proc. Natl. Acad. Sci.* ***109***, 12974–12979 (2012).

253 12. S. R. K. Vedula *et al.*, Epithelial bridges maintain tissue integrity during collective cell migration.
254 *Nat. Mater.* ***13***, 87–96 (2014).

255 13. C. Leclech, D. Gonzalez-Rodriguez, A. Villedieu, T. Lok, A.-M. Déplanche, A. I. Barakat,
256 Topography-induced large-scale antiparallel collective migration in vascular endothelium. *Nat.*
257 *Commun.* ***13***, 2797 (2022).

258 14. J. Park *et al.*, Switch-like enhancement of epithelial-mesenchymal transition by YAP through
259 feedback regulation of WT1 and Rho-family GTPases. *Nat. Commun.* ***10***, 2797 (2019).

260 15. B. Sarker, A. Bagchi, C. Walter, J. Almeida, A. Pathak, Longer collagen fibers trigger multicellular
261 streaming on soft substrates via enhanced forces and cell–cell cooperation. *J. Cell Sci.* ***132***,

262 jcs226753 (2019).

263 16. T. Greeshma *et al.*, Cell contact guidance via sensing anisotropy of network mechanical
264 resistance. *Proc. Natl. Acad. Sci.* ***118***, e2024942118 (2021).

265 17. A. S. Keys, A. R. Abate, S. C. Glotzer, D. J. Durian, Measurement of growing dynamical length
266 scales and prediction of the jamming transition in a granular material. *Nat. Phys.* ***3***, 260–264
267 (2007).

268 18. V. Trappe, V. Prasad, L. Cipelletti, P. N. Segre, D. A. Weitz, Jamming phase diagram for attractive
269 particles. *Nature*. ***411***, 772–775 (2001).

270 19. A. J. Liu, S. R. Nagel, Jamming is not just cool any more. *Nature*. ***396***, 21–22 (1998).

271 20. L. Atia *et al.*, Geometric constraints during epithelial jamming. *Nat. Phys.* ***14***, 613–620 (2018).

272 21. A. J. Liu, S. R. Nagel, The Jamming Transition and the Marginally Jammed Solid. *Annu. Rev.*
273 *Condens. Matter Phys.* ***1***, 347–369 (2010).

274 22. C. Malinverno *et al.*, Endocytic reawakening of motility in jammed epithelia. *Nat. Mater.* ***16***, 587–
275 596 (2017).

276 23. F. Giavazzi *et al.*, Flocking transitions in confluent tissues. *Soft Matter*. ***14***, 3471–3477 (2018).

277 24. D. T. Tambe *et al.*, Collective cell guidance by cooperative intercellular forces. *Nat. Mater.* ***10***,
278 469–475 (2011).

279 25. D. T. Tambe *et al.*, Collective cell guidance by cooperative intercellular forces. *Nat. Mater.* ***10***,
280 469–475 (2011).

281 26. X. Serra-Picamal *et al.*, Mechanical waves during tissue expansion. *Nat. Phys.* ***8***, 628–634 (2012).

282 27. A. Saraswathibhatla, J. Zhang, J. Notbohm, Coordination of contractile tension and cell area
283 changes in an epithelial cell monolayer. *Phys. Rev. E*. ***105***, 24404 (2022).

284 28. S. A. Gudipaty *et al.*, Mechanical stretch triggers rapid epithelial cell division through Piezo1.
285 *Nature*. ***543***, 118–121 (2017).

286

287

288 ## Acknowledgements:

289 The authors acknowledge technical assistance and equipment sharing by Dr. James Quirk for using MRI
290 strength magnet and Professor Vijay Ramani for the use of vacuum filtration and rota-evaporator. This
291 work was supported by the NIH/NIGMS grant R35GM128764 (to AP) and National Science Foundation,
292 Science and Technology Centers, Center for Engineering MechanoBiology grant CMMI:154857 (to AP
293 and MF).

Author Contributions

AB and AP conceived the project and designed study. AB performed experiments and computational modeling, analyzed data, interpreted findings, made figures, and wrote the manuscript. BS, JZ and MF contributed methods and reagents for polyacrylamide gel synthesis. AP edited the manuscript, supervised the project, and acquired funding.

Conflicts of Interest

The authors declare no competing interests.

Data Availability

Source codes used for data analysis and plotting figures are available on reasonable request.

Figures

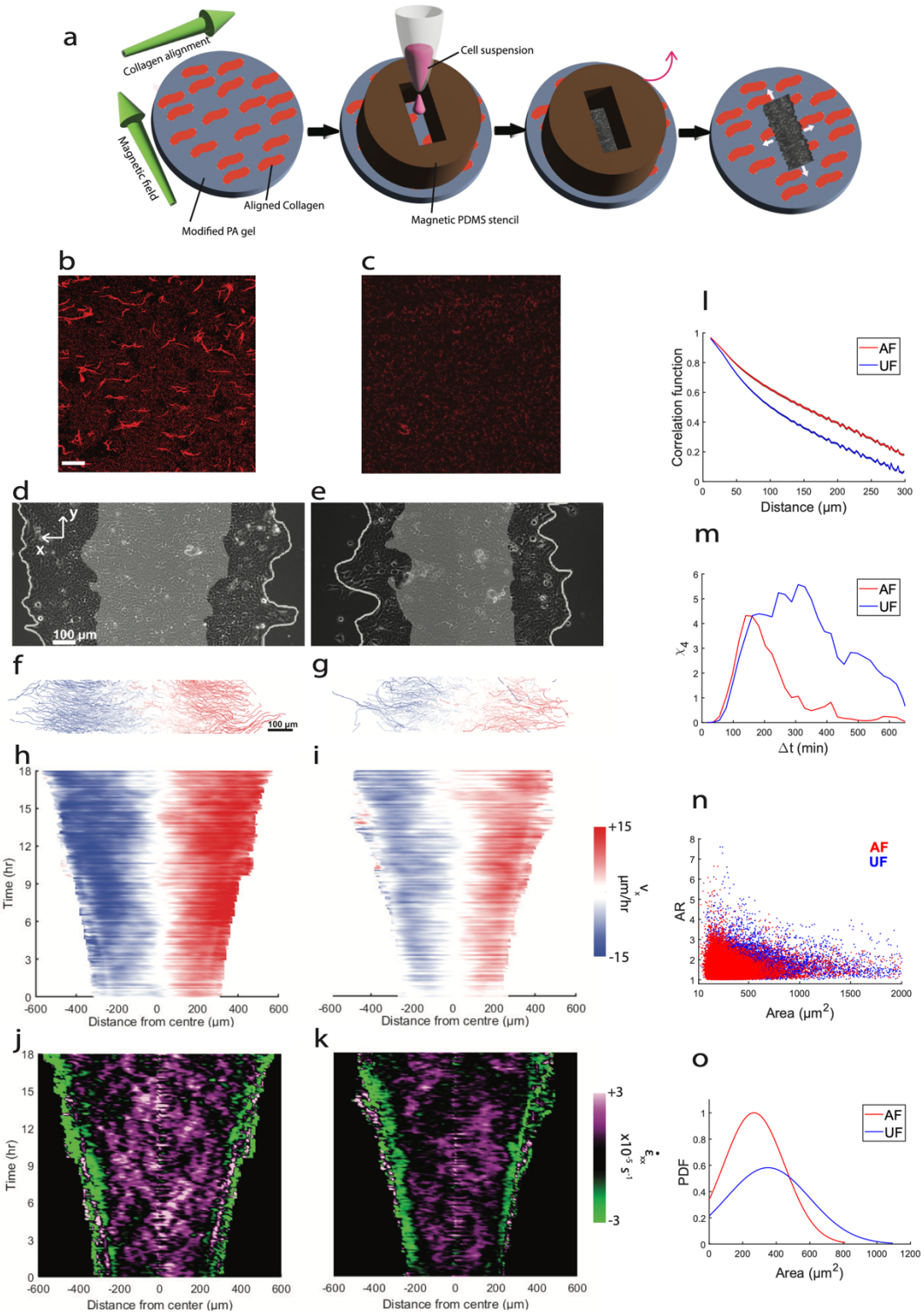

Figure 1. Aligned fibers cause faster and more directed motion within cell clusters. (**a**) Modified soft polyacrylamide (mod-PA) gels are exposed to high strength magnetic field to orient collagen in particular

direction. A PDMS stencil is deposited on the mod-PA gel. MCF-10A cells are seeded and allowed to attach only by the gap defined by PDMS stencil. When cells reach confluency, stencil is lifted, and cells start invading available space. Representative images of fluorescently labelled collagen-1 on AF (**b**) and UF (**c**). Scale bar is 50 µm. (**d**) A representative monolayer expanding on aligned fiber gels (AF). Gray transparent region indicates monolayer's initial position (t = 0 hours). Phase contrast shows the monolayer at 16hours. Gray lines indicate monolayer edges. (**e**) Example of monolayer expanding on uniform fiber gels (UF). (**f** and **g**) Individual cell trajectories corresponding to experiments shown in (d) and (e) respectively. Color-coding shows mean cell speed in x-direction for every track. Kymographs of cell velocity component in x-direction (v_x) (**h** and **i**), velocity strain rate $\dot{\varepsilon}_x$ (**j** and **k**) corresponding to experiments shown in (d) and (e) respectively. (**l**) Time-averaged (m = 157) spatial autocorrelation function of v_x for AF (red) and UF (blue) for n = 3 observations, error is represented as standard error. (**m**) The four-point susceptibility χ_4 as a function of Δt for AF (red) and UF (blue). (**n**) Scatter plots of cell aspect ratio (AR) versus cellular area for AF (56117 cells, red) and UF (39447 cells, blue). (**o**) Distribution of cellular area for cells on AF (red) and UF (blue).

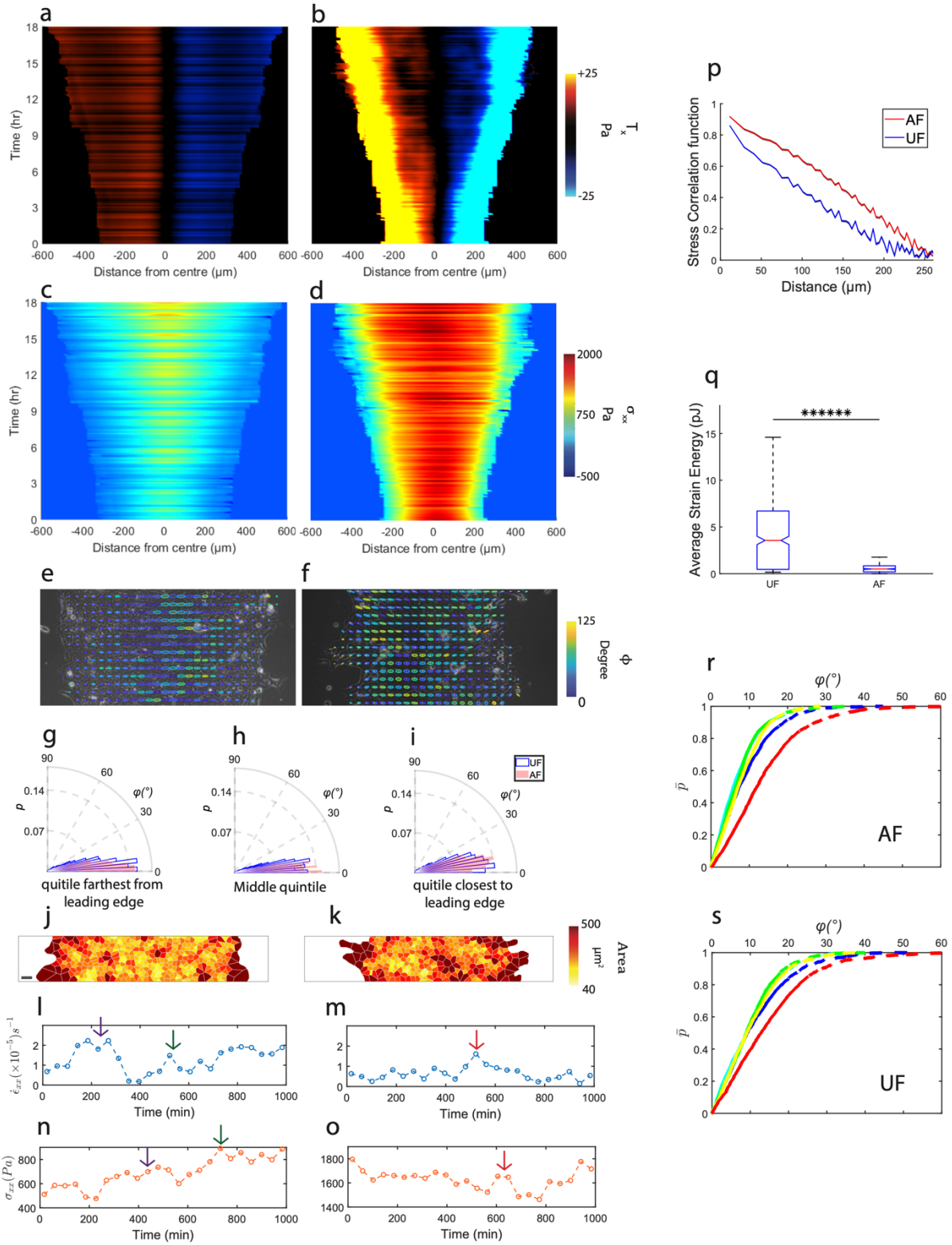

Figure 2. Aligned fibers reduces traction forces and monolayer stresses within migrating cell clusters causing a force effective mode of migration. (**a** and **b**) Kymographs for traction component T_x for AF (a)

and UF (b). (**c** and **d**) Kymographs for monolayer stress component σ_{xx}. (**e** and **f**) Principal stress ellipse overlaid on phase contrast images for monolayer on AF (e) and UF (f). Stress ellipse are color coded according to alignment angle φ between major axis of principle stress ellipse and direction of cellular velocity. (**g**-**i**) Alignment angle φ comparison between AF and UF at quintiles farthest (g), mid-distance (h) and closest (i) to the leading edge. In all three cases, distribution is narrower for AF indicating that "plithotaxis" is more dominant in AF compared to UF. (**j** and **k**) Polygons approximating cell shapes for monolayer on AF (j) and UF (k). Polygons are color coded corresponding to area. (**l** and **m**) Average value of $\dot{\varepsilon}_{xx}$ for AF (**l**) and UF (**m**) and σ_{xx} for AF (**n**) and UF (**o**). For curves in (l),(m),(n) and (o), four consecutive values were averaged for curve smoothening purposes. (**p**) Time averaged (m = 157) spatial correlation function of average-normal stresses in AF (red) and UF (blue) for n = 3 observations, error is represented as standard error. (**q**) Strain energy imparted by monolayer on AF and UF averaged across entire duration of migration (m = 157) across n = 3 (***** P = 1.98 x 10^{-84}). (**r**) Cumulative probability distribution $\bar{P}(\varphi)$ curves, from red to blue are at decreasing distance from leading edge for monolayer migrating on AF. (**s**) Cumulative probability distribution for monolayer migrating on UF. Each curve in (**r**) and (**s**) and distribution in (g), (h) and (i) have more than 1000 values.

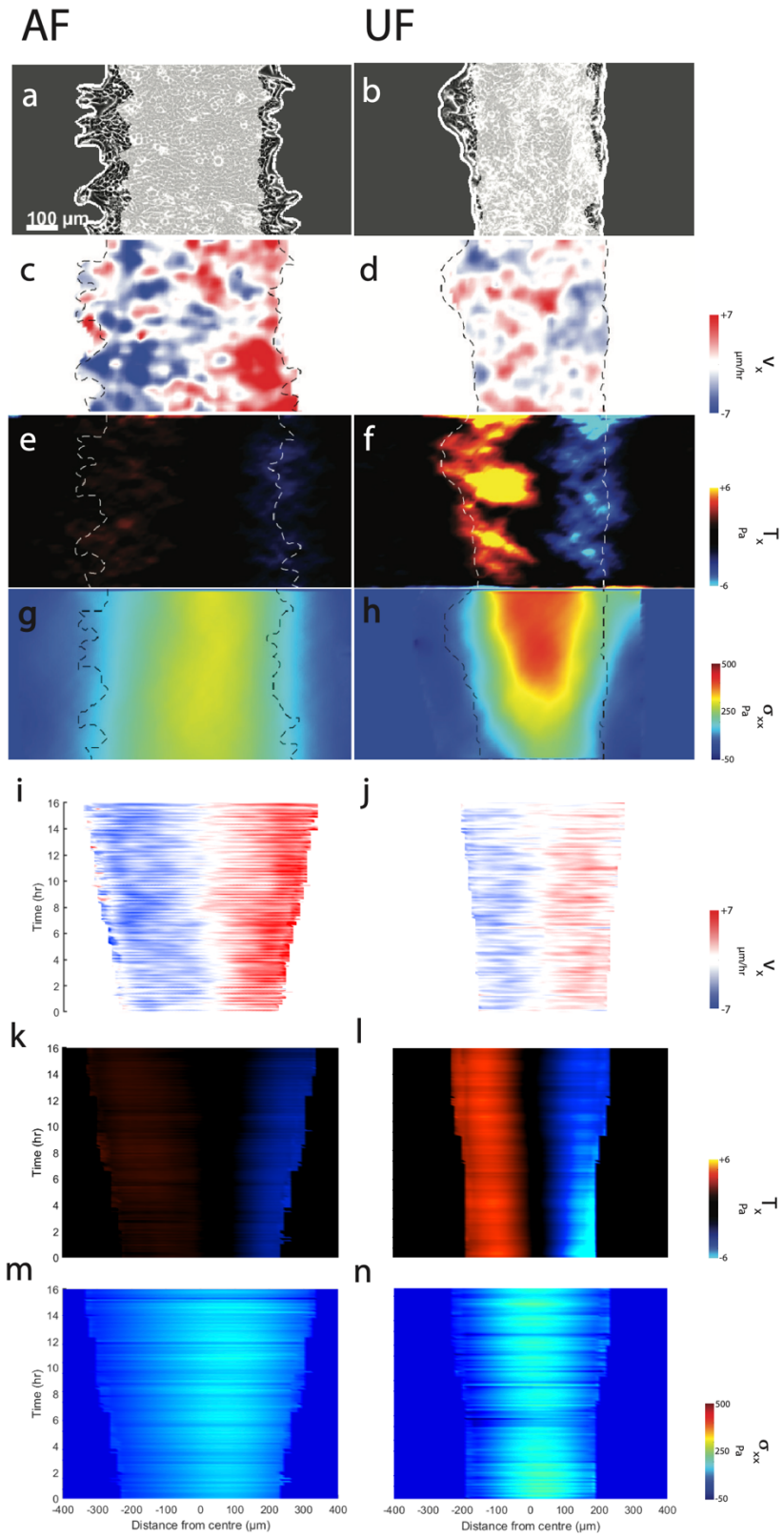

Figure 3. Reducing substrate stiffness maintains faster force effective migration phenotype on AF when compared to UF. (**a** and **b**) Phase contrast images of cell monolayer migrating of softer AF (a) and

softer UF (b). (**c** and **d**) Maps of velocity component v_x. (**e** and **f**) Maps of traction component T_x. (**g** and **h**) Maps of monolayer stress component σ_{xx}. (**i** and **j**) Kymographs of velocity component v_x for cell monolayer migrating of softer AF (a) and softer UF (b). (**k** and **l**) Kymographs of traction component T_x. (**m** and **n**) Kymographs of monolayer stress component σ_{xx}.

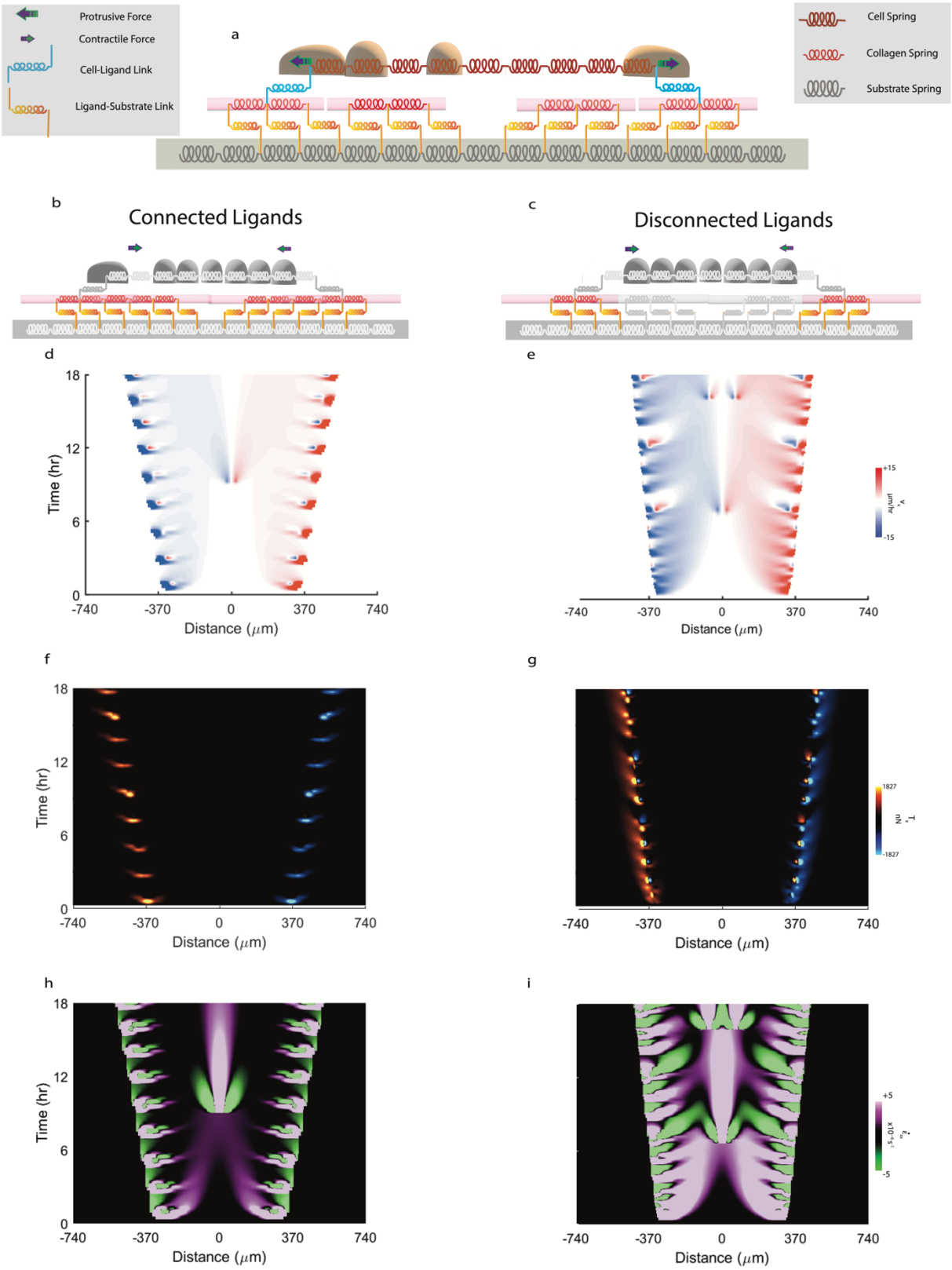

Figure 4. Physical model shows that fiber connectivity leads to rapid contractility stabilization leading to fast force-effective migration mode (**a**) Schematic of one-dimensional in-silico model of a line of

epithelial cells represented by springs sliding viscously over rigid ligand springs which are fixed to substrate springs after a self-propelling force is acted upon at the leader nodes. (**b**) and (**c**) represent how connected ligands and disconnected ligands are modelled in-silico. In connected ligand condition (b), higher number of ligand-substrate bonds get engaged during contractility driven retraction of monolayer compared to disconnected condition (c). (**d** and **e**) In-silico velocity kymograph for connected ligands (d) and disconnected ligands (e). (**f** and **g**) In-silico traction force kymograph for connected ligands (f) and disconnected ligands (g). (**h** and **i**) In-silico strain-rate kymograph for connected ligands (h) and disconnected ligands (i).